Image force on a charged projectile moving over a two-dimensional strongly coupled Yukawa system

Lu-Jing Hou and Z. L. Mišković
Department of Applied Mathematics, University of Waterloo, Waterloo, Ontario, Canada N2L 3G1
(Received 25 October 2007; published 2 April 2008)

We use both analytical theory and numerical simulations to study the image force on a charged particle moving parallel to a two-dimensional strongly coupled Yukawa system. Special attention is paid to the effects of strong correlation and nonlinear response in the Yukawa system on the dependences of the image force on the particle velocity and its distance from the Yukawa system. Those effects are elucidated by comparing the results obtained from a Brownian dynamics simulation with those from linear-dielectric-response theories based on both the quasilocalized charge approximation and the standard Vlasov random phase approximation.

DOI: 10.1103/PhysRevE.77.046401 PACS number(s): 52.40.Hf, 52.25.Vy, 52.35.Fp

I. INTRODUCTION

When a charged particle is in the proximity of a boundary surface between two media—for example, between the air and a conductor or dielectric—a charge density (or polarization) will be induced on the boundary surface, giving rise to the so-called image force on the particle [1]. The image interaction continues to play important roles in the development of surface science—e.g., in surface tunneling microscopy [2] and in studies of the electron image states on solid surfaces [3] or around carbon nanotubes [4].

In the present article, we study the interactions of an external charge with a two-dimensional (2D) assembly of strongly coupled particles repelling each other in the pairwise manner via the Yukawa-like potential of the form $\phi(r)=[(Ze)^2/r]\exp(-r/\lambda)$, with Z being the charge number on each particle, $e>0$ the elementary charge, λ the (Debye) screening length, and r the in-plane interparticle distance. Such a Yukawa system is often used in studying the dynamics of 2D colloidal crystals [5,6]. It may be also regarded as a simplified model for several recent experiments involving dusty plasmas [7–13], where charged dust particles are levitated and confined in the plasma sheath due to a strong electric field in that region, forming typically a monolayer of the so-called plasma crystal or, in some instances, also quasi-3D crystals with just a few layers [14]. In some of those experiments, the focus was placed on external charged particles moving parallel to the dust layers [7,9–11], and we take up here the task of exploring the image force on such particles resulting from the dynamic polarization of a monolayer of dust particles. This task is of fundamental interest because it presents a theoretical recognition and analysis of the image interaction within the context of strongly coupled 2D Yukawa systems, but it also offers a promising aid to understanding the related experiments [7,9–14], in particular, the interactions among—and the stability of—multiple layers of dust particles in plasmas, as well as the issues regarding the orbital stability of external charges moving near dust monolayers. Specifically, we shall explore variations of the image force with the relevant system parameters such as the coupling parameter within the dust layer, as well as the speed and distance of the external particle from that layer. Comparison of the results for the image force obtained from the Brownian dynamics (BD) simulation with those of linear-response theories will aid us in highlighting the strong-correlation and the nonlinear response effects of the dust layer.

A 2D Yukawa system is well characterized by the coupling parameter $\Gamma=(Ze)^2/(aT)$ and the screening parameter $\kappa=a/\lambda$, where T is the system temperature (in energy units) and $a=(\pi\sigma_0)^{-1/2}$ is the average interparticle distance, or the so-called 2D Wigner-Seitz radius, with σ_0 being the equilibrium density per unit area of the 2D Yukawa system. For convenience, we introduce here two additional parameters: the *nominal* plasma frequency ω_p and the sound speed v_s, which are defined, respectively, by $\omega_p=(\frac{2\pi e^2Z^2\sigma_0}{m\lambda})^{1/2}$ with m being the mass of particles and $v_s=\omega_p a$. We shall be using the so-called test charge formalism, which was first introduced in Refs. [15,16] in the context of the wake field in weakly coupled plasma. Thus, we refer to the external charge as the test particle (TP), assuming that it carries Z_t elementary charges and moves with constant velocity $\mathbf{v}$ parallel to the dust layer at a constant distance h, as shown in Fig. 1. The potential Φ_{ext} by which the TP interacts with individual particles in the dust layer immersed in a plasma sheath is not well understood at present, mostly because of the unclear role of the asymmetry in the potential Φ_{ext} brought up by the ion flow in the sheath and the related wake effects [15–17].

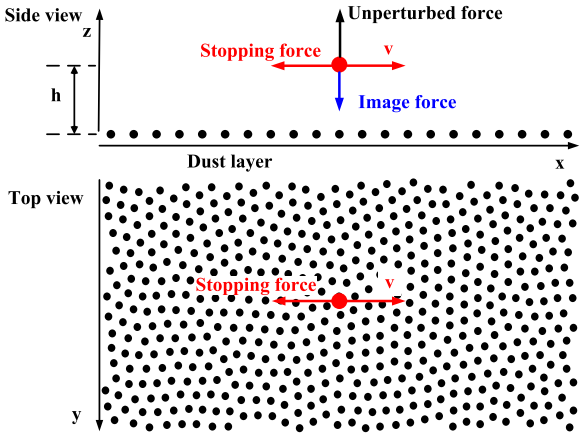

FIG. 1. (Color online) Schematic diagram for the model system and the definition of the image force on test particle.

While the use of the Yukawa model is well justified for the interparticle interaction potential $\phi(r)$ within the dust layer in directions parallel to the sheath boundary [8], a fully self-consistent determination of the potential Φ_{ext} should be performed, taking into account the ion-wake effects. Postponing this task for a future work, we shall assume here Φ_{ext} to be an isotropic, 3D Yukawa-like potential with the same screening length λ as in the interparticle potential $\phi(r)$ within the layer (we shall be also using $Z_t=Z$ in all calculations), thereby disregarding the ion flow in the plasma sheath [21,22]. While such an assumption simplifies the analysis in the present work, it nevertheless has its merits for at least two purposes: (a) unambiguous identification and estimation of the order of magnitude of the image force in dusty plasmas and (b) achieving broader interest, e.g., in the context of 2D colloidal systems where the ion flow usually does not play any significant role [5,6].

A 2D Yukawa system may be treated as a dielectric medium. In that context, a moving charged TP inevitably polarizes a dust layer, giving rise to a collective response which often exhibits excitations of the dust-acoustic waves. If the interaction with the TP is weak enough, the polarization of the dust layer can be treated within the linear dielectric-response formalism [15,16], upon which our analytical models are based. As a consequence of this polarization, the TP experiences forces which may be viewed as arising from the collective effects of displacements of dust particles in the longitudinal directions across the layer. The force component acting in the direction parallel to the dust layer and opposing the motion of the TP is called the *stopping force*, and it was studied in detail elsewhere [22]. On the other hand, the *image force* acts in the direction perpendicular to the dust layer and pulls the TP toward that layer. Unlike the stopping force, the image force does not vanish when the TP is stationary, but rather usually attains its largest values for stationary TPs. Of course, the image force is counteracted by a repulsive force which is obtained as the sum of the repulsive Yukawa-like interactions between the TP and individual dust particles taken over their unperturbed positions within the layer.

After outlining the analytical theory used to evaluate the image force based on the quasilocalized charge approximation (QLCA), we shall briefly describe the method used for measuring the perpendicular force from our BD simulation. The subsequent presentation of the results and their comparative analysis will be followed by a summary of our findings.

II. ANALYTICAL THEORY

We adopt a macroscopic point of view in which the whole dust layer is regarded as a continuous 2D medium whose response to the external electromagnetic disturbances may be fully characterized by its dielectric response, while the microscopic details of the interparticle interactions and the structure of the layer may be incorporated through an appropriate model dielectric function. So, to take into account the short-range correlation effects within the dust layer, we use in our analysis mainly the QLCA method due to Kalman and Golden [18–20], which has been found to be very successful in describing the collective phenomena in strongly coupled dusty plasmas [19–22].

Consider a dust layer in the $z=0$ plane of a Cartesian coordinate system with $\mathbf{R}=\{\mathbf{r},z\}$ where $\mathbf{r}=\{x,y\}$, and a TP moving with a constant velocity $\mathbf{v}$ parallel to the dust layer at a constant distance $h>0$. Polarization of charges in the layer will give rise to the induced electric potential $\Phi_{ind}(\mathbf{r},z,t)$, which is related to the electric potential of the TP, $\Phi_{ext}(\mathbf{r},z,t)$, within linear-response theory, as follows: $\Phi_{ind}(\mathbf{k},k_z,\omega)=[\varepsilon_L^{-1}(\mathbf{k},\omega)-1]\Phi_{ext}(\mathbf{k},k_z,\omega)$, where we have used the Fourier transform with respect to space, $\mathbf{R}\equiv\{\mathbf{r},z\}\rightarrow\mathbf{K}\equiv\{\mathbf{k},k_z\}$, and time, $t\rightarrow\omega$, variables. Here, $\varepsilon_L(\mathbf{k},\omega)$ is the longitudinal dielectric response function of the 2D dust layer which may be expressed as [23,24]

$$\varepsilon_L(\mathbf{k},\omega)=1-\frac{\omega_0^2(k)}{\omega(\omega+i\gamma)-\frac{\sigma_0}{m}G(\mathbf{k},\omega)}, \tag{1}$$

where

$$\omega_0^2(k)=\frac{\sigma_0}{m}\phi(k)k^2,$$

with

$$\phi(k)=\frac{2\pi(Ze)^2}{(k^2+\lambda^{-2})^{1/2}}$$

being the 2D Fourier transform of the Yukawa potential $\phi(r)$. Here, γ is a phenomenological damping factor (Epstein coefficient) accounting for the dust-neutral collisions in dusty plasmas and $G(\mathbf{k},\omega)$ is the so-called dynamic local field correction (DLFC) function, introduced to account for the short-range correlation effects beyond the mean-field random-phase-approximation (RPA) description [23,24]. Note that setting $G(\mathbf{k},\omega)=0$ simply recovers the RPA dielectric function in the so-called plasmon pole approximation.

Since it is difficult to construct the DLFC directly, we adopt here its static form of the local field correction from the QLCA method, in which $\frac{\sigma_0}{m}G(\mathbf{k},\omega\rightarrow\infty)\equiv D_L(\mathbf{k})$, with $D_L(\mathbf{k})$ being the longitudinal projection of the 2D QLCA dynamical matrix. The function $D_L(\mathbf{k})$ may be expressed in terms of the equilibrium radial distribution function (RDF) of the dust layer, $g(\mathbf{r})$, as follows [19–22]:

$$D_L(k)=\frac{\omega_p^2\lambda}{2}\int_0^\infty dr\frac{g(r)-1}{r^2}\exp\left(-\frac{r}{\lambda}\right)\left[\left(1+\frac{r}{\lambda}+\frac{r^2}{\lambda^2}\right)-\left(4+\frac{4r}{\lambda}+\frac{2r^2}{\lambda^2}\right)J_0(kr)+\left(6+\frac{6r}{\lambda}+\frac{2r^2}{\lambda^2}\right)\frac{J_1(kr)}{kr}\right], \tag{2}$$

where J_0 and J_1 are the Bessel functions of the first kind. It is clear that the evaluation of Eq. (2) requires an input for the RDF, $g(r)$, which will be determined numerically from the BD simulation.

Next, by applying the inverse Fourier transform, one obtains the induced potential

$$\Phi_{ind}(\mathbf{r},z,t) = \frac{eZ_t\omega_p^2\lambda}{2\pi}\int d^2\mathbf{k}\frac{(k\lambda)^2\exp[-\frac{|z|+h}{\lambda}\sqrt{1+(k\lambda)^2}+i\mathbf{k}\cdot(\mathbf{r}-\mathbf{v}t)]}{[1+(k\lambda)^2]H_L(k,\mathbf{k}\cdot\mathbf{v})}, \tag{3}$$

where $H_L(k,\mathbf{k}\cdot\mathbf{v})=[\omega(\omega+i\gamma)-D_L(\mathbf{k})]\varepsilon_L(\mathbf{k},\mathbf{k}\cdot\mathbf{v})$. One can obtain, in a similar fashion, also the expressions for the perturbed density distribution and the perturbed velocity field of dust particles within the layer, which typically show Mach-cone structure, as has been shown in our previous work [21]. However, we are concerned here with the image force acting on the TP, which is directly related to the induced potential through the definition

$$F_{im}(v,h) \equiv -eZ_t\left.\frac{\partial\Phi_{ind}}{\partial z}\right|_{\mathbf{r}=\mathbf{v}t,z=h} = \frac{(eZ_t)^2\omega_p^2}{2\pi}\int d^2\mathbf{k}\frac{(k\lambda)^2\exp[-\frac{2h}{\lambda}\sqrt{1+(k\lambda)^2}]}{\sqrt{1+(k\lambda)^2}H_L(k,\mathbf{k}\cdot\mathbf{v})}. \tag{4}$$

Note that, unlike the stopping force from our previous study [22], F_{im} is a *conservative* force because it can be written as $F_{im}=-\partial V_{im}/\partial h$ where $V_{im}(v,h)$ is the image potential of the TP, defined by $V_{im}=\frac{1}{2}eZ_t\Phi_{ind}(\mathbf{r}=\mathbf{v}t,z=h)$. For example, in the RPA limit ($D_L=0$) with no screening ($\lambda\to\infty$) and for a static ($v=0$) TP, we obtain from Eq. (4) the force $F_{im}=-e^2Z_t^2/(4h^2)$, which is just the negative of the derivative of the well-known image potential of a point charge eZ_t a distance h from a perfectly conducting plane, $V_{im}=-e^2Z_t^2/(4h)$, resulting from Eq. (3) under the same conditions ($D_L=0$, $\lambda\to\infty$, $v=0$).

III. NUMERICAL RESULTS

To be consistent with our previous study of energy losses of TPs moving parallel to dust layers, we use here the same parameters as those in Ref. [22]. Specifically, we consider the dusty argon plasma with the parameters selected according to the relevant experiments [7]: bulk plasma density $n_0=1.0\times10^8$ cm^3; electron temperature $T_e=3.0$ eV; equal temperatures for the plasma ions and the dust-particle system, $T_i=T=0.1$ eV; mass density of dust particles, $\rho_d=1.0$ g/cm^3; and their radius $r_d=2.0$ μm. Under these conditions, we obtain $\lambda=231$ μm. We have found that variations in the discharge pressure p play no substantial role in our simulations, so we fix it at the typical value of $p=20$ Pa [7], giving for the Epstein drag coefficient $\gamma=25$ s^{-1}. We consider a range of Γ values covering a phase transition from liquid to crystal, while keeping $\kappa=1$ (and, consequently, $a=231$ μm) throughout present simulations, so that the dust charge Z varies in the range from $-1260e$ to $-4000e$ depending on Γ. While keeping the TP charge fixed at $Z_t=Z$, we vary its speed v and its height h above the dust layer, which both determine the strength of the TP coupling with the dust layer, to be discussed in Figs. 3 and 5.

A. Description of the simulation

Charged dust particles interact with each other via the Yukawa potential $\phi(r)$, with the strength of interaction fully characterized by Γ and κ, and are simultaneously exposed to random forcing due to asymmetric molecular bombardment by the neutral gas, giving rise to a Brownian component in the motion of each dust particle. Our simulation is based on the BD method [25–27] in which we track the Brownian motions of a number of dust particles in a rectangle with the periodic boundary conditions. While the details of the algorithm will be discussed elsewhere, we give here only an outline of our simulation, which consists of two steps. Initially, no external perturbation is applied to the system, which consists of $N=1600$ charged particles being initially placed at random positions in the computational domain. They then undergo Brownian motions while interacting with each other, until the system reaches the equilibrium. This calculation reveals some dynamical properties of the system, such as the phonon spectra and the dispersion relations for collective modes, as well as some static properties, such as the RDF which is then used as an input for the QLCA model in Eq. (2). In the second step (after the system has reached the equilibrium), a TP carrying Z_t elementary charges, is projected into the system at a constant distance h from the dust layer. Without losing generality, we assume here that the TP moves on a straight line along the x direction with constant velocity $\mathbf{v}$, as shown in Fig. 1.

The details of the interactions between the TP and all particles in the dust layer are recorded giving, e.g., the wave excitation patterns and their propagation in the layer, as well as their relaxation after the perturbation ceases. In particular, the total force $\mathbf{F}_t$ exerted on the TP by the dust particles is measured directly. In order to obtain the image force, we first record the perpendicular component of the total force, $F_\perp \equiv \hat{\mathbf{z}}\cdot\mathbf{F}_t$. To show how this measurement works, we give in Fig. 2(a) several samples of the direct measurements of $F_\perp$ as a function of the position x when the TP moves at several speeds from the left to the right over the computational domain (for clarity, we do not show the whole range of these measurements in Fig. 2). Note that, hereafter, the speed of the TP is normalized by v_s which depends on Γ, while the force is normalized by $F_n=T_e/\lambda$, in the same way as was the stopping force normalized in Ref. [22]. We see that the force is not only a (random) function of x, but is also velocity dependent. The quasi-oscillatory behavior of the forces seen in Fig. 2(a) is attributed mainly to the discrete structure of the dust distribution within the layer, as one can conclude from similarity of the curves obtained at different speeds. The TP experiences forces from all particles in the dust layer; however, those particles at the shortest distances from the TP—i.e., those participating in "head-on" collisions with the TP—normally contribute the most. As a consequence, the

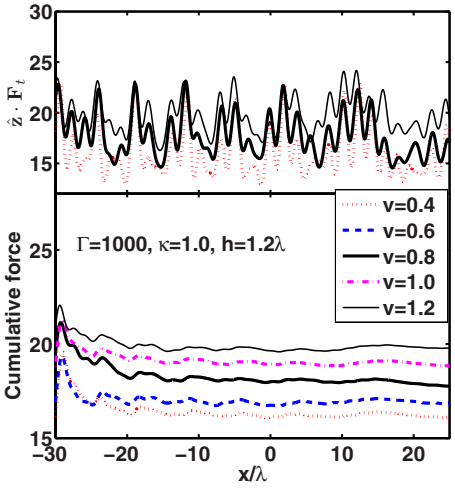

FIG. 2. (Color online) BD measurements of the total perpendicular force (in units of $F_n=T_e/\lambda$) versus the reduced position x/λ for (upper panel) the force itself for three speeds of the test particle (curves from bottom up), $v=0.4$, 0.8, and 1.2 (in units of $v_s=3.09$ cm/s), and for (lower panel) the cumulative force for five speeds of the test particle (curves from bottom up), $v=0.4$, 0.6, 0.8, 1.0, and 1.2 (in units of $v_s=3.09$ cm/s), with fixed $\Gamma=1000$, $\kappa=1$, $h=1.2\lambda$, and $Z_t=Z$.

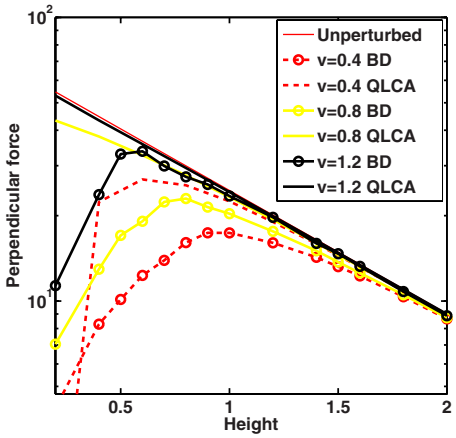

FIG. 3. (Color online) The dependence of the total perpendicular force (in units of $F_n=T_e/\lambda$) on the height of the test particle above the dust layer h (in units of λ), obtained from the BD simulation (chained curves) and the QLCA model (corresponding unchained curves), for three speeds of the test particle (curves from bottom up): $v=0.4$, 0.8, and 1.2 (in units of $v_s=3.09$ cm/s), with fixed $\Gamma=1000$, $\kappa=1$, and $Z_t=Z$. The topmost straight thin line shows the unperturbed force F_0 (in units of F_n).

"peaks" seen in the oscillations of forces shown in Fig. 2(a) are approximately related to the positions of such "head-on" encounters. This picture is quite similar to that occurring in the scanning force microscope (SFM) measurements, where the tip is moving over a solid surface, giving information on the surface structure which is reflected in the force (including the image force) acting on the tip [28]. However, in a real dusty plasma experiment, this position-dependent behavior of the perpendicular force could be very difficult to observe. What one could measure, however, are the mean values of these forces. Namely, one expects $F_\perp(x)$ to be a stationary (and ergodic) stochastic process for a given speed, so one can evaluate the cumulative force over the path of length x, as follows from $\frac{1}{x}\int_0^x F_\perp(x')dx'$, and register its value after large enough x, giving thus an approximation to the mean of $F_\perp$. In Fig. 2(b) we show several samples of the cumulative force evaluated in this way, which are all seen to approach steady, velocity-dependent values after the TP has traversed a long enough path.

In Fig. 3 we display by the chain curves the thus measured mean *perpendicular force* $F_\perp$ versus the distance h for several TP speeds. The straight thin solid line shows the case based on the measurements of the force on a moving TP when the perturbation of the dust layer is artificially neglected; we thus refer to this force as the *unperturbed force* $F_0(h)$. Note that this repulsive force is actually independent of the TP speed. We have found it to be well fitted, regardless of the actual structure of the dust layer, by the analytical result

$$F_0 = 2\pi Z_t Z e^2 \sigma_0 \exp(-h/\lambda), \tag{5}$$

obtained from a superposition of the Yukawa-like potentials between the TP and the dust particles when they are assumed to be continuously distributed within the layer. However, when the perturbation of the dust layer by the TP is allowed for in our simulation, the force dependence on the distance h is quite different from the exponentially decaying unperturbed force $F_0(h)$. One notices in Fig. 3 that the repulsive character of the total measured perpendicular force weakens as the TP moves closer to the dust layer, eventually reaching zero when the TP is in the layer (not shown in this figure), so that effectively $F_\perp$ passes through a broad, velocity-dependent maximum at distances on the order of the interparticle spacing a within the layer. Such behavior is a consequence of the rearrangements of the dust particles, or the polarization of the dust layer by the moving TP, which gives rise to an attractive component in the measured $F_\perp$ when the TP is close to the layer. Thus, the difference $F_0-F_\perp$—i.e., the *unperturbed force* minus the total *perpendicular force*—gives the magnitude of the *image force* from our BD simulation.

B. Comparison with analytical models

In Fig. 3 we also show, by the unchained curves, the results for the total force F_0+F_{im}, where F_0 is evaluated from Eq. (5) and the image force F_{im} from Eq. (4) in the QLCA model with the RDFs obtained from the same sets of the BD simulations as those used to measure the perpendicular forces $F_\perp$, shown by the corresponding chain curves in the same figure. One notices in Fig. 3 very large discrepancies between the numerical and analytical results, especially when the TP is close to the dust layer, which point to the possibly very strong nonlinear effects in the dust-layer response. We therefore concentrate in the following on comparisons between the results for the image force obtained from the BD simulation and those obtained from both the QLCA and RPA models. We shall specifically consider the

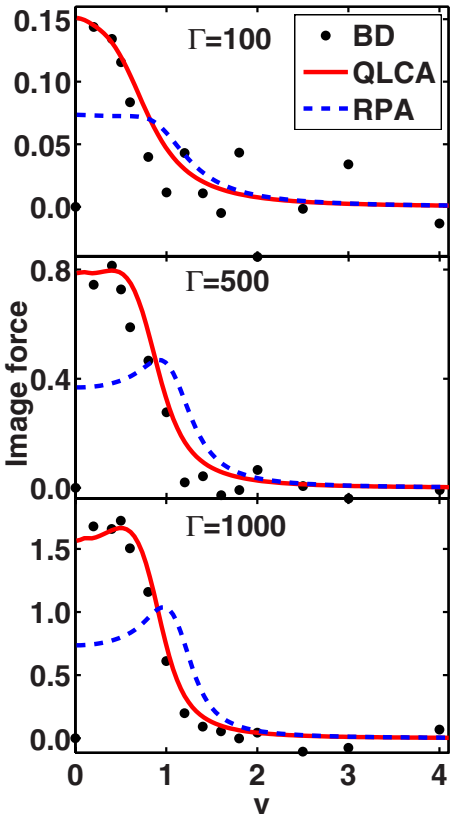

FIG. 4. (Color online) Magnitude of the image force (in units of $F_n=T_e/\lambda$) versus the speed of the test particle v (in units of v_s), obtained from the BD simulation (dots), the QLCA model (solid curves), and the RPA model (dashed curves), for three coupling strengths (panels from top to bottom): $\Gamma=100$, 500, and 1000 (giving, respectively, the sound speeds of $v_s=0.98$, 2.18, and 3.09 cm/s), with fixed $\kappa=1$, $Z_t=Z$, and $h=1.5\lambda$.

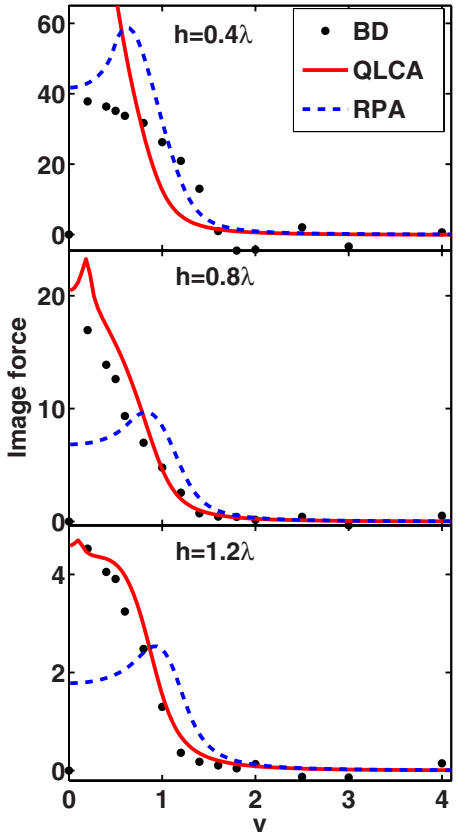

FIG. 5. (Color online) Magnitude of the image force (in units of $F_n=T_e/\lambda$) versus the speed of the test particle v (in units of $v_s=3.09$ cm/s), obtained from the BD simulation (dots), the QLCA model (solid curves), and the RPA model (dashed curves), for three distances of the test particle to the dust layer (panels from top to bottom): $h=0.4\lambda$, 0.8λ, and 1.2λ, with fixed $\Gamma=1000$, $\kappa=1$, and $Z_t=Z$.

velocity dependence of the image force for several values of the coupling strength and the TP distance, in order to reveal the effects of both the strong correlation and the nonlinear response in the dust layer.

In Fig. 4 we show the magnitude of the image force versus the TP speed v for several coupling strengths Γ and with the fixed distance $h=1.5\lambda$. A general feature shown by all curves in Fig. 4 is that the image force is most pronounced in the region of low speeds and quickly diminishes at high speeds, with the transition region being around the sound speed v_s. This can be understood by the fact that at low speeds the dust layer has enough time to respond (through displacements of the dust particles) to the perturbation caused by the moving TP and consequently undergoes a stronger polarization for slower TPs and vice versa. Another important feature revealed in Fig. 4 is that the results from the RPA method are increasingly inadequate as the coupling strength increases, as expected, especially at speeds below the sound speed. On the other hand, one can notice in Fig. 4 a very good agreement between the simulation results and the curves obtained from the QLCA method for all speeds and all coupling strengths shown in that figure, indicating that the QLCA method successfully captures the strong-coupling effect. However, it should be pointed out that this success of the QLCA method, being a linear theory, hinges on the relatively large distance h used in Fig. 4, which guarantees that the TP exerts a sufficiently weak perturbation on the dust layer. Nonlinear effects are expected to become increasingly significant in the image force when the charge of the TP increases and/or when its distance from the dust layer decreases.

In Fig. 5 we show the magnitude of the image force versus the TP speed v for several distances h and with fixed coupling strength of $\Gamma=1000$. One notices in the figure that, while the QLCA results agree quite closely with the simulation data at all speeds for the distance $h=1.2\lambda$, as in Fig. 4, and somewhat less closely for the intermediate distance of $h=0.8\lambda$, this agreement deteriorates spectacularly when the TP moves at the shortest distance displayed, $h=0.4\lambda$, for practically all speeds which yield a sizable image force for that case. (Interestingly, the RPA seems to give a better agreement, possibly fortuitously, with the BD data than the QLCA does for the lowest speeds, as well as for the intermediate speeds—say, $v_s<v<2v_s$—in the case of the shortest distance h shown in Fig. 5.) While an obvious explanation stems from the fact that the QLCA method is essentially a linear theory, one can pinpoint the direct cause of the QLCA's failure as being its use of the *equilibrium* RDF in Eq.

(4). Namely, at $h=0.4\lambda=0.4a$, with a being the average interparticle distance within the dust layer, the perturbation brought by the TP to that layer is so strong that the concept of a RDF for the dust layer is no longer justified locally. We have found similar effects of short distances in our previous simulations of the stopping force on moving TPs, pointing to the same conclusion [22].

In order to address the nonlinear effects in a more quantitative manner, we define a parameter, the projectile-target coupling strength Θ, which characterizes the interaction between the TP and dust particles and is defined by $\Theta=V_{td}/(V_{dd}+mv^2/2)$, similar to the definition given in Ref. [29], where $V_{td}=|Z_tZ|e^2\exp(-h/a)/h$ is the maximum of the interaction energy between the TP and a dust particle, and $V_{dd}=Z^2e^2\exp(-\kappa)/a$ is the average pairwise interaction energy within the dust layer. Considering the criterion for a weak coupling to be $\Theta \ll 1$, one may explain well the regions of good agreement between the QLCA results and the BD data for the image force observed in Figs. 4 and 5.

IV. SUMMARY

We have presented a combined analytical and numerical analysis of the image force on a charged particle moving over a two-dimensional strongly coupled Yukawa system, representing typical experimental configurations involving dust layers in the plasma sheath regions. The dependences of the image force on the coupling strength, projectile speed, and its distance from such a layer are discussed in detail. Comparisons of the results derived from two analytical models, the RPA and the QLCA, with those of the BD simulation revealed several important features of the image force. Good agreement between the QLCA results and the BD simulation is found in the parameter range where conditions for a weak perturbation are met, primarily requiring large enough distances between the projectile and the dust layer and/or high enough projectile speeds. On the other hand, agreement between the RPA results and the BD simulation is observed only for very high projectile speeds, where both effects of strong correlation and nonlinear response are not significant.

Besides its fundamental interest in analyzing the dynamic polarization of strongly coupled Yukawa systems, this study also points to the need of including the image force in future simulations which will consider full dynamics of the projectile motion. Namely, a simple analysis of our expression (4) for the image force shows that, in the linear-response regime, its order of magnitude is $F_{im}\sim(eZ/\lambda)^2$, which is comparable to most of the other forces occurring in dusty plasmas, such as the average screened electrostatic interparticle force, the ion-wake force [15–17], and the ion-drag force [see, e.g., Eq. (6) and Fig. 1 in Ref. [30]], as well as the so-called shadow force [see, e.g., Eq. (1) and the text above it in Ref. [31], and references therein], all sharing the same order of magnitude, $(eZ/\lambda)^2$. However, it should be stressed that, for a real 2D dusty plasma formed in a plasma sheath, calculations of the image force should examine how the asymmetry in the test-particle potential Φ_{ext} due to the ion wake, which was neglected in the present calculation, affects the polarization of a dust layer. While we do not expect significant differences in the order of magnitude of the image force on test particles, in future work we shall undertake a more elaborate determination of this force in the presence of an ion wake in the potential Φ_{ext} due to ion flow in a plasma sheath [15–17], which may reveal novel and interesting qualitative features in the image force, not present in condensed matter systems [2,3].

ACKNOWLEDGMENTS

This work was supported by NSERC and PREA (Z.L.M.). L.J.H. would like to thank Professor You-Nian Wang for useful discussion.

[1] J. D. Jackson, *Classical Electrodynamics*, 3rd ed. (Wiley, New York, 1998), Chap. 2.
[2] J. M. Blanco, F. Flores, and R. Perez, Prog. Surf. Sci. **81**, 403 (2006).
[3] T. Fauster, M. Weinelt, and V. Hofer, Prog. Surf. Sci. **82**, 224 (2007).
[4] B. E. Granger, P. Kral, H. R. Sadeghpour, and M. Shapiro, Phys. Rev. Lett. **89**, 135506 (2002); M. Zamkov, N. Woody, B. Shan, H. S. Chakraborty, Z. Chang, U. Thumm, and P. Richard, *ibid.* **93**, 156803 (2004).
[5] F. M. Peeters and X. Wu, Phys. Rev. A **35**, 3109 (1987).
[6] A. Libal, C. Reichhardt, and C. J. Olson Reichhardt, Phys. Rev. E **75**, 011403 (2007).
[7] D. Samsonov, J. Goree, Z. W. Ma, A. Bhattacharjee, H. M. Thomas, and G. E. Morfill, Phys. Rev. Lett. **83**, 3649 (1999).
[8] U. Konopka, G. E. Morfill, and L. Ratke, Phys. Rev. Lett. **84**, 891 (2000).
[9] V. A. Schweigert, I. V. Schweigert, V. Nosenko, and J. Goree, Phys. Plasmas **9**, 4465 (2002).
[10] R. Ichiki, Y. Ivanov, M. Wolter, Y. Kawai, and A. Melzer, Phys. Rev. E **70**, 066404 (2004).
[11] Y. Ivanov and A. Melzer, Phys. Plasmas **12**, 072110 (2005).
[12] S. Nunomura, S. Zhdanov, D. Samsonov, and G. Morfill, Phys. Rev. Lett. **94**, 045001 (2005).
[13] S. Nunomura, D. Samsonov, S. Zhdanov, and G. Morfill, Phys. Rev. Lett. **96**, 015003 (2006).
[14] J. H. Chu and L. I, Phys. Rev. Lett. **72**, 4009 (1994); H. Thomas, G. E. Morfill, V. Demmel, J. Goree, B. Feuerbacher, and D. Mohlmann, *ibid.* **73**, 652 (1994); Y. Hayashi and K. Tachibana, Jpn. J. Appl. Phys., Part 2 **33**, L804 (1994); A. Melzer, T. Trottenberg, and A. Piel, Phys. Lett. A **191**, 301 (1994).
[15] M. Nambu, S. V. Vladimirov, and P. K. Shukla, Phys. Lett. A **203**, 40 (1995).
[16] P. K. Shukla and N. N. Rao, Phys. Plasmas **3**, 1770 (1996).
[17] L. J. Hou, Y. N. Wang, and Z. L. Mišković, Phys. Rev. E **64**, 046406 (2001).
[18] G. J. Kalman and K. I. Golden, Phys. Rev. A **41**, 5516 (1990);

K. I. Golden and G. J. Kalman, Phys. Plasmas **7**, 14 (2000).
[19] G. J. Kalman, M. Rosenberg, and H. E. DeWitt, Phys. Rev. Lett. **84**, 6030 (2000).
[20] G. J. Kalman, P. Hartmann, Z. Donkó, and M. Rosenberg, Phys. Rev. Lett. **92**, 065001 (2004).
[21] K. Jiang, L. J. Hou, Y. N. Wang, and Z. L. Mišković, Phys. Rev. E **73**, 016404 (2006).
[22] L. J. Hou, Z. L. Mišković, K. Jiang, and Y. N. Wang, Phys. Rev. Lett. **96**, 255005 (2006).
[23] M. S. Murillo and D. O. Gericke, J. Phys. A **36**, 6273 (2003).
[24] S. Ichimaru, H. Iyetomi, and S. Tanaka, Phys. Rep. **149**, 91 (1987).
[25] M. P. Allen and D. J. Tildesley, *Computer Simulation of Liquids* (Oxford University Press, New York, 1989), Chap. 9.
[26] D. S. Lemons, *An Introduction to Stochastic Processes in Physics* (Johns Hopkins University Press, Baltimore, 2002), Chaps. 7 and 8.
[27] X. H. Zheng and J. C. Earnshaw, Phys. Rev. Lett. **75**, 4214 (1995).
[28] L. N. Kantorovich, A. S. Foster, A. L. Shluger, and A. M. Stoneham, Surf. Sci. **445**, 283 (2000); L. N. Kantorovich, A. L. Shluger, and A. M. Stoneham, Phys. Rev. Lett. **85**, 3846 (2000).
[29] G. Zwicknagel, C. Toepffer, and P. G. Reinhard, Phys. Rep. **309**, 117 (1999).
[30] A. V. Ivlev, S. A. Khrapak, S. K. Zhdanov, G. E. Morfill, and G. Joyce, Phys. Rev. Lett. **92**, 205007 (2004).
[31] V. N. Tsytovich, N. G. Gousein-zade, and G. E. Morfill, Phys. Plasmas **13**, 033503 (2006).